Int. J. Heat Mass Transfer. Vol. 31, No. 5, pp. 1063–1072, 1988
Printed in Great Britain

0017–9310/88 $3.00+0.00

Application of elliptic grid generation technique to the solution of hydrodynamics and heat transfer of droplet arrays at intermediate Reynolds numbers

STEVEN J. CHEN and ALBERT Y. TONG
Mechanical Engineering Department, University of Texas at Arlington, Arlington, TX 76019, U.S.A.

(*Received* 15 *April* 1987 *and in final form* 20 *October* 1987)

Abstract—The objective of the present study is to employ the numerical grid generation technique for the solution of hydrodynamics and heat transfer in a three-droplet array. Elliptic partial differential equations are used to generate grids in the physical plane. The Navier–Stokes equations in vorticity–stream-function form and the energy equation have been solved numerically by the finite difference method for the Reynolds number range of 10–200. Numerical solutions in terms of drag coefficient and Nusselt number have been obtained. The results are compared with the results obtained in an earlier study as well as those in the literature.

1. INTRODUCTION

THE THEORY of fuel droplet vaporization and spray combustion has been under development for several decades. During recent years it has received a large amount of attention. Most studies on the combustion of liquid fuel sprays consider the vaporization of either single isolated droplets or overall droplet sprays, and relatively few works have been carried out on interactions between droplets.

In dense spray situations, many droplets are present, and the average distance between droplets can be as low as a few droplet diameters. It is expected that the geometry and scale of the diffusion field surrounding each individual droplet will be affected by the droplet interaction. The Nusselt number and the functional form of the relationship between vaporization rates and local ambient conditions will be influenced by the droplet spacing.

Some investigators have examined a few droplets in a well-defined geometry or a large number of droplets in a periodic configuration. These arrangements are sometimes referred to as droplet arrays. These arrays, although artificial, can be very useful in obtaining information on the effect of droplet spacing on transport rates. Some work on hydrodynamics and heat transfer to an array of spheres with forced convection has been performed by Tal *et al.* [1, 2]. In these studies, an infinite array of spheres of radius '*a*' with uniform spacing '2*b*' (Fig. 1) is considered. Due to symmetry and the nearly periodic character associated with an infinite array, no heat transfer or momentum transfer takes place at the streamwise equidistant plane between the spheres. By this assumption, the problem is reduced to a multitude of spheres in tandem in a square streamtube (Fig. 2) which is subsequently replaced with a cylindrical duct of equal cross-sectional area. A three-sphere array is subsequently used.

The Navier–Stokes equations in vorticity–stream-function form and the energy equation are solved numerically by using a finite difference method with non-uniform cylindrical mesh. The diffusion terms are expressed using a central difference scheme and the convection terms (in both the vorticity and the energy equation) using an upwind difference scheme.

Recently, the present authors [3] extended Tal *et al.*'s formulation to the vaporizing droplet case. Nusselt number correlations for both the vaporizing and the non-vaporizing droplet cases have been obtained. In order to reduce the amount of false diffusion caused by an upwind difference scheme, a hybrid scheme is used instead. It is realized that there is one drawback to the non-uniform cylindrical mesh geometry. It does not have a uniformly fine grid around the droplet surface region. Therefore, the accuracy of the solution will be affected by the relatively coarser grids in spite of the finer spacings in some other regions.

In order to eliminate the disadvantage of the non-uniform cylindrical mesh and to improve the numerical accuracy, a numerical grid generation technique is used in the present study. Numerical grid generation has been widely used for a numerical solution of partial differential equations in arbitrarily shaped regions. Numerous advantages accrue when this technique is employed. For example, the body surface can be selected as a boundary in the computational plane so that the complication of boundary shape is effectively removed from the problem. It is also possible to distribute the transformed coordinate lines in the

NOMENCLATURE

a	radius of droplet
$2b$	distance between the centers of two neighboring droplets
c_d	total drag coefficient
C_{df}	friction drag coefficient
C_{dp}	pressure drag coefficient
C_p	specific heat at constant pressure
d	diameter of droplet, $2a$
h	heat transfer coefficient
J	Jacobian of transformation
k	thermal conductivity
Nu	Nusselt number, hd/k
Pr	Prandtl number, $C_p\mu/k$
r, ϕ, z	cylindrical coordinates
Re	Reynolds number, $V_i d/\nu$
T	dimensionless temperature, $(T'-T'_s)/(T'_i-T'_s)$
T'	temperature
T'_i	inlet temperature
T'_s	droplet surface temperature
u	dimensionless velocity in z-direction
v	dimensionless velocity in r-direction
V_i	inlet velocity
x	dimensionless axial coordinate, z/a
X	value of x at outlet
y	dimensionless radial coordinate, r/a.

Greek symbols

α	thermal diffusivity
θ	angle from frontal stagnation point
μ	dynamic viscosity
ν	kinematic viscosity
ξ, η	transformed coordinates
ρ	density
ψ	dimensionless stream function, $\psi'/V_i a^2$
ψ'	stream function
ω	dimensionless vorticity, $\omega' a/V_i$
ω'	vorticity.

Subscripts

i	inlet
n	normal to the droplet surface
s	droplet surface
0	frontal stagnation point.

Superscripts

	dimensional quantity
-	averaged quantity.

physical plane with concentration of lines on regions of high gradients while maintaining the square grid in the computational plane.

Some work on using numerical grid generation for a single droplet study has been carried out by Patnaik [4]. In the present study, elliptic partial differential equations are used to generate grids for the three-droplet array configuration. Numerical solutions of partial differential equations are done on the transformed coordinate system by transforming all partial derivatives analytically so that the transformed coordinates, rather than the physical coordinates, become the independent variables. The result is a set of partial differential equations and boundary conditions in which all derivatives are with respect to the transformed coordinates. These equations are then expressed as finite difference equations on the square grid that is inherent in the transformed plane. The governing equations, expressed as difference equations in the computational plane, are solved by a successive line underrelaxation method.

Although the present study focuses on the non-vaporizing droplet array case, the formulation can be extended to the vaporizing droplet situation. Nusselt numbers and drag coefficients have been obtained for intermediate Reynolds numbers (Re = 10–200). The results are compared with the results of the previous work [3] as well as those in ref. [1].

The details of the grid generation are explained in Section 2. In Section 3, the mathematical formulations which have been derived in ref. [3] are presented for completeness. The finite difference forms of the governing equations are derived in Section 4 followed by results and discussion.

2. THE GRIDS

The problem of grid generation is that of determining the mapping which takes the grid points from the physical domain to the computational domain. Various schemes are available to achieve such mappings, including conformal mappings, algebraic schemes and elliptic partial differential equations. Thompson *et al.* [5] have worked extensively on using elliptic partial differential equations to generate grids. This mapping is constructed by specifying the desired grid points (x, y) on the boundary of the physical domain. The distribution of points on the interior is then determined by solving

$$\xi_{xx}+\xi_{yy} = P(\xi,\eta)$$
$$\eta_{xx}+\eta_{yy} = Q(\xi,\eta) \quad (1)$$

where (ξ, η) represent the coordinates in the computational domain and P and Q are terms which control the point spacing on the interior of the physical domain. The effect of changing the functions P and Q on the coordinate system is discussed by Thompson *et al.* [6]. One particularly effective procedure is to choose P and Q as exponential terms so that the coordinates are generated as the solutions of

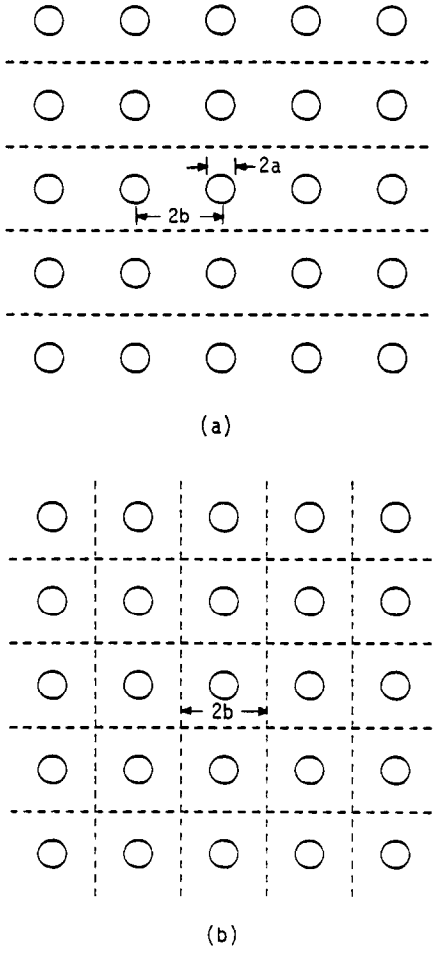

FIG. 1. Assemblage geometry: (a) side view; (b) front view (after ref. [1]).

$$\xi_{xx}+\xi_{yy} = -\sum_{i=1}^{n} a_i \operatorname{sgn}(\xi-\xi_i)\exp(-c_i|\xi-\xi_i|) - \sum_{j=1}^{m} b_j \operatorname{sgn}(\xi-\xi_j)\exp(-d_j((\xi-\xi_j)^2 + (\eta-\eta_j)^2)^{1/2}) \equiv P(\xi,\eta) \quad (2a)$$

$$\eta_{xx}+\eta_{yy} = -\sum_{i=1}^{n} a_i' \operatorname{sgn}(\eta-\eta_i)\exp(-c_i'|\eta-\eta_i|) - \sum_{j=1}^{m} b_j' \operatorname{sgn}(\eta-\eta_j)\exp(-d_j'((\xi-\xi_j)^2 + (\eta-\eta_j)^2)^{1/2}) \equiv Q(\xi,\eta). \quad (2b)$$

The first terms have the effect of attracting the ξ = constant lines to the $\xi = \xi_i$ lines in equation (2a), and attracting η = constant lines to the $\eta = \eta_i$ lines in equation (2b). The second terms cause ξ = constant lines to be attracted to the points (ξ_j, η_j) in equation (2a), with a similar effect on η = constant lines in equation (2b).

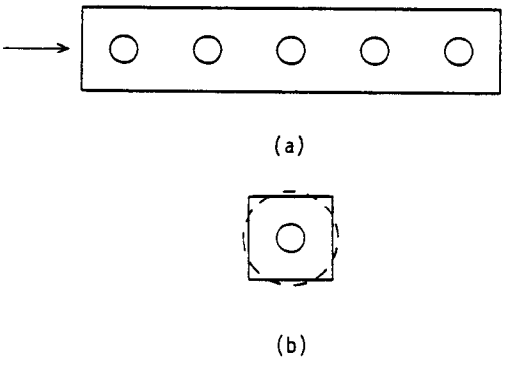

FIG. 2. Multisphere cylindrical cell: (a) side view; (b) front view (after ref. [1]).

Elliptic partial differential equations are used to generate grids in the present study. All derivatives are approximated by second order central differences. The set of non-linear difference equations is solved by successive line overrelaxation.

The magnitude of the range of the transformed coordinates, ξ and η, is irrelevant to the subsequent use of the coordinate system in the numerical solution of partial differential equations, for the mesh widths in the transformed plane, $\Delta\xi$ and $\Delta\eta$, simply cancel out from all difference expressions for transformed derivatives. Therefore, $\Delta\xi$ and $\Delta\eta$ are both taken as unity for convenience, with ξ and η each ranging from unity to the total number of coordinate lines of each description.

Figure 3 shows the surface-oriented coordinates obtained as a solution of the transformation for a three-droplet array. A non-uniform distribution of points has been obtained in the physical domain, while the computational domain is maintained with a uniform rectangular grid.

It should be mentioned that the slab corners in the transformed field are special points which require special treatment. This type of special point occurs when a convex corner in the transformed field is associated with a point on a smooth contour in the physical field. Both coordinate lines experience slope discontinuities at this point (Fig. 4). In the present study, a linear distribution of partial derivatives in the neighborhood of a special point has been assumed. Other techniques for treating the special point can be found in ref [6].

3. MATHEMATICAL FORMULATION

The governing equations for the axisymmetric flow field and heat transfer in cylindrical coordinates have been derived in the previous paper [3] and are summarized here for completeness

$$\omega = \frac{1}{y}\left[\frac{\partial^2\psi}{\partial x^2} + \frac{\partial^2\psi}{\partial y^2} - \frac{1}{y}\frac{\partial\psi}{\partial y}\right] \quad (3)$$

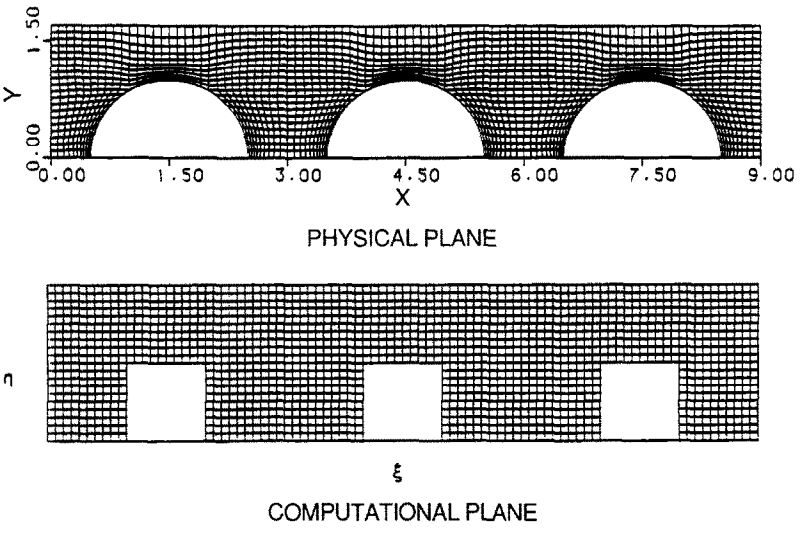

FIG. 3. Mapping to computational space.

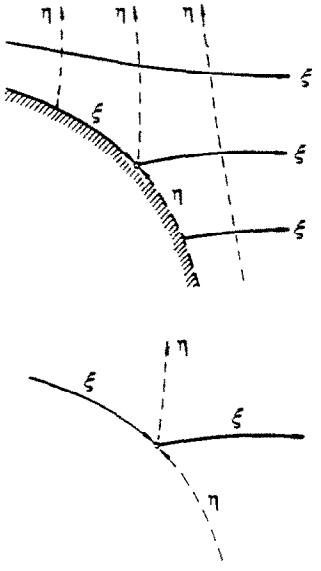

FIG. 4. Slope discontinuities at special point (after ref. [6]).

$$\frac{Re}{2y}\left[\frac{\partial\psi}{\partial y}\frac{\partial\omega}{\partial x}-\frac{\partial\psi}{\partial x}\frac{\partial\omega}{\partial y}\right]+\frac{Re\,\omega}{2y^2}\frac{\partial\psi}{\partial x}=\frac{\partial^2\omega}{\partial x^2}+\frac{\partial^2\omega}{\partial y^2}+\frac{1}{y}\frac{\partial\omega}{\partial y}-\frac{\omega}{y^2} \quad (4)$$

$$\frac{Re\,Pr}{2y}\left[\frac{\partial\psi}{\partial y}\frac{\partial T}{\partial x}-\frac{\partial\psi}{\partial x}\frac{\partial T}{\partial y}\right]=\frac{\partial^2 T}{\partial x^2}+\frac{\partial^2 T}{\partial y^2}+\frac{1}{y}\frac{\partial T}{\partial y} \quad (5)$$

where the stream function, ψ, is defined as

$$u=\frac{1}{y}\frac{\partial\psi}{\partial y} \quad (6)$$

$$v=-\frac{1}{y}\frac{\partial\psi}{\partial x}. \quad (7)$$

The boundary conditions are:

(i) at the inlet, $x = 0$

$$\psi=\tfrac{1}{2}y^2$$
$$\omega=0$$
$$T=1; \quad (8)$$

(ii) at the axis of symmetry, $y = 0$

$$\psi=0$$
$$\omega=0$$
$$\frac{\partial T}{\partial y}=0; \quad (9)$$

(iii) at the outlet, $x = X$

$$\frac{\partial\psi}{\partial x}=0$$
$$\frac{\partial\omega}{\partial x}=0$$
$$\frac{\partial T}{\partial x}=0; \quad (10)$$

(iv) at the cylinder wall, $y = (b/a)\,(4/\pi)^{1/2}$

$$\psi=\frac{2}{\pi}\left(\frac{b}{a}\right)^2$$
$$\omega=0$$
$$\frac{\partial T}{\partial y}=0; \quad (11)$$

(v) at the droplet surface

$$\psi=0$$
$$\omega=\frac{\partial u}{\partial y}-\frac{\partial v}{\partial x}$$
$$T=0. \quad (12)$$

In boundary condition (v), the vorticity at the drop-

let surface is calculated following its definition. The velocity components are obtained from differentiating the stream function following equations (6) and (7).

As mentioned in ref. [3], the above formulation is valid for the non-vaporizing droplet case. It was found by Prakash [7] that the surface velocity is typically small and does not affect the heat and mass transfers or the vaporization rate in the gas phase. Because of that the surface velocity can be neglected in the gas-phase analysis. This greatly simplifies the problem by eliminating the matching of the surface velocity along the droplet surface. The model also assumed that the temperature at the droplet surface remains constant and uniform.

The local heat transfer to the droplet can be expressed in terms of the local Nusselt number which is given by

$$Nu_\theta = 2\frac{\partial T}{\partial n}. \tag{13}$$

Subsequently, the overall average heat transfer to the whole droplet can be expressed as

$$\overline{Nu} = \frac{1}{2}\int_0^\pi Nu_\theta \sin\theta \, d\theta. \tag{14}$$

As for the drag coefficients, the derivations for friction drag and pressure drag can be found in Jenson [8]. They are given by

$$C_{df} = \frac{8}{Re}\int_0^\pi \omega \sin^2\theta \, d\theta \tag{15}$$

$$C_{dp} = \int_0^\pi P_\theta \sin 2\theta \, d\theta \tag{16}$$

where

$$P_\theta = P_0 + \frac{4}{Re}\int_0^\theta \left(\frac{\partial \omega}{\partial n} + \omega\right) d\theta. \tag{17}$$

The governing equations as well as the boundary conditions are expressed in finite difference form in conjunction with the numerical elliptic grid generation technique. The details are given in the next section.

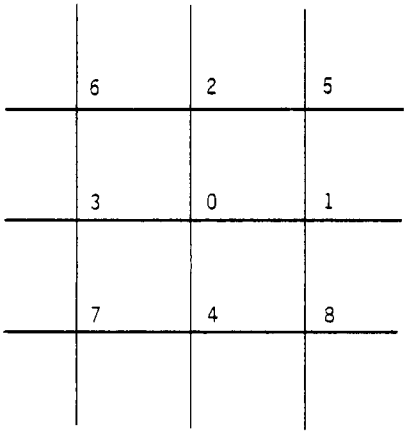

FIG. 5. Grid numbering system.

4. FINITE DIFFERENCE FORMULATION

In order that the computations can be performed on a rectangular grid in the computational plane, it is convenient to transform the governing equations from the physical domain (x, y) to the computational domain (ξ, η). Using the chain rule of partial differentiation the partial derivatives become

$$\begin{aligned}
\frac{\partial}{\partial x} &= \xi_x \frac{\partial}{\partial \xi} + \eta_x \frac{\partial}{\partial \eta} \\
\frac{\partial}{\partial y} &= \xi_y \frac{\partial}{\partial \xi} + \eta_y \frac{\partial}{\partial \eta} \\
\frac{\partial^2}{\partial x^2} &= \xi_{xx}\frac{\partial}{\partial \xi} + \eta_{xx}\frac{\partial}{\partial \eta} + \xi_x^2 \frac{\partial^2}{\partial \xi^2} + \eta_x^2 \frac{\partial^2}{\partial \eta^2} \\
&\quad + 2\xi_x\eta_x \frac{\partial^2}{\partial \xi \, \partial \eta} \\
\frac{\partial^2}{\partial y^2} &= \xi_{yy}\frac{\partial}{\partial \xi} + \eta_{yy}\frac{\partial}{\partial \eta} + \xi_y^2 \frac{\partial^2}{\partial \xi^2} + \eta_y^2 \frac{\partial^2}{\partial \eta^2} \\
&\quad + 2\xi_y\eta_y \frac{\partial^2}{\partial \xi \, \partial \eta}.
\end{aligned} \tag{18}$$

The matrices $(\xi_x, \xi_y, \eta_x, \eta_y, \xi_{xx}, \xi_{yy}, \eta_{xx}, \eta_{yy})$ appearing in these equations are obtained from the following expressions:

$$\begin{aligned}
\xi_x &= \frac{y_\eta}{J} \\
\xi_y &= \frac{-x_\eta}{J} \\
\eta_x &= \frac{-y_\xi}{J} \\
\eta_y &= \frac{x_\xi}{J} \\
\xi_{xx} &= \frac{x_\eta(y_{\xi\xi}\xi_x^2 + 2y_{\xi\eta}\xi_x\eta_x + y_{\eta\eta}\eta_x^2) - y_\eta(x_{\xi\xi}\xi_x^2 + 2x_{\xi\eta}\xi_x\eta_x + x_{\eta\eta}\eta_x^2)}{J} \\
\xi_{yy} &= \frac{x_\eta(y_{\xi\xi}\xi_y^2 + 2y_{\xi\eta}\xi_y\eta_y + y_{\eta\eta}\eta_y^2) - y_\eta(x_{\xi\xi}\xi_y^2 + 2x_{\xi\eta}\xi_y\eta_y + x_{\eta\eta}\eta_y^2)}{J} \\
\eta_{xx} &= \frac{y_\xi(x_{\xi\xi}\xi_x^2 + 2x_{\xi\eta}\xi_x\eta_x + x_{\eta\eta}\eta_x^2) - x_\xi(y_{\xi\xi}\xi_x^2 + 2y_{\xi\eta}\xi_x\eta_x + y_{\eta\eta}\eta_x^2)}{J} \\
\eta_{yy} &= \frac{y_\xi(x_{\xi\xi}\xi_y^2 + 2x_{\xi\eta}\xi_y\eta_y + x_{\eta\eta}\eta_y^2) - x_\xi(y_{\xi\xi}\xi_y^2 + 2y_{\xi\eta}\xi_y\eta_y + y_{\eta\eta}\eta_y^2)}{J}
\end{aligned} \tag{19}$$

Referring to the notation of the rectangular ξ–η grid of Fig. 5, the following central difference approximations are used:

$$\left.\frac{\partial F}{\partial \xi}\right|_0 = \frac{F_1 - F_3}{2}$$

$$\left.\frac{\partial F}{\partial \eta}\right|_0 = \frac{F_2 - F_4}{2}$$

$$\left.\frac{\partial^2 F}{\partial \xi\, \partial \eta}\right|_0 = \frac{F_5 - F_6 + F_7 - F_8}{4}$$

$$\left.\frac{\partial^2 F}{\partial \xi^2}\right|_0 = F_1 + F_3 - 2F_0$$

$$\left.\frac{\partial^2 F}{\partial \eta^2}\right|_0 = F_2 + F_4 - 2F_0. \tag{20}$$

Here F is a generalized function representing T, ψ, ω, x or y. Substituting equations (18)–(20) into equation (3), followed by some rearrangement, leads to the following equation:

$$C_0\psi_0 = C_1\psi_1 + C_2\psi_2 + C_3\psi_3 + C_4\psi_4 + C_5(\psi_5 - \psi_6 + \psi_7 - \psi_8) - \omega_0 \tag{21}$$

where

$$C_0 = \frac{2}{y}(\xi_x^2 + \xi_y^2 + \eta_x^2 + \eta_y^2)$$

$$C_1 = \frac{1}{2y}\left(\xi_{xx} + \xi_{yy} - \frac{1}{y}\xi_y\right) + \frac{1}{y}(\xi_x^2 + \xi_y^2)$$

$$C_2 = \frac{1}{2y}\left(\eta_{xx} + \eta_{yy} - \frac{1}{y}\eta_y\right) + \frac{1}{y}(\eta_x^2 + \eta_y^2)$$

$$C_3 = -\frac{1}{2y}\left(\xi_{xx} + \xi_{yy} - \frac{1}{y}\xi_y\right) + \frac{1}{y}(\xi_x^2 + \xi_y^2)$$

$$C_4 = -\frac{1}{2y}\left(\eta_{xx} + \eta_{yy} - \frac{1}{y}\eta_y\right) + \frac{1}{y}(\eta_x^2 + \eta_y^2)$$

$$C_5 = \frac{1}{2y}(\xi_x\eta_x + \xi_y\eta_y). \tag{22}$$

Similarly, equation (4) becomes

$$D_0\omega_0 = D_1\omega_1 + D_2\omega_2 + D_3\omega_3 + D_4\omega_4 + D_5(\omega_5 - \omega_6 + \omega_7 - \omega_8) \tag{23}$$

where

$$D_0 = 2(\xi_x^2 + \xi_y^2 + \eta_x^2 + \eta_y^2) - \frac{Re\, v}{2y} + \frac{1}{y^2}$$

$$D_1 = \frac{1}{2}\left(\xi_{xx} + \xi_{yy} + \frac{1}{y}\xi_y\right) + (\xi_x^2 + \xi_y^2) - \frac{1}{2}\left(\frac{Re}{2}\xi_x u + \frac{Re}{2}\xi_y v\right)$$

$$D_2 = \frac{1}{2}\left(\eta_{xx} + \eta_{yy} + \frac{1}{y}\eta_y\right) + (\eta_x^2 + \eta_y^2) - \frac{1}{2}\left(\frac{Re}{2}\eta_x u + \frac{Re}{2}\eta_y v\right)$$

$$D_3 = -\frac{1}{2}\left(\xi_{xx} + \xi_{yy} + \frac{1}{y}\xi_y\right) + (\xi_x^2 + \xi_y^2) + \frac{1}{2}\left(\frac{Re}{2}\xi_x u + \frac{Re}{2}\xi_y v\right)$$

$$D_4 = -\frac{1}{2}\left(\eta_{xx} + \eta_{yy} + \frac{1}{y}\eta_y\right) + (\eta_x^2 + \eta_y^2) + \frac{1}{2}\left(\frac{Re}{2}\eta_x u + \frac{Re}{2}\eta_y v\right)$$

$$D_5 = \frac{1}{2}(\xi_x\eta_x + \xi_y\eta_y) \tag{24}$$

and equation (5) becomes

$$E_0T_0 = E_1T_1 + E_2T_2 + E_3T_3 + E_4T_4 + E_5(T_5 - T_6 + T_7 - T_8) \tag{25}$$

where

$$E_0 = 2(\xi_x^2 + \xi_y^2 + \eta_x^2 + \eta_y^2)$$

$$E_1 = \frac{1}{2}\left(\xi_{xx} + \xi_{yy} + \frac{1}{y}\xi_y\right) + (\xi_x^2 + \xi_y^2) - \frac{1}{2}\left(\frac{Re\,Pr}{2}\xi_x u + \frac{Re\,Pr}{2}\xi_y v\right)$$

$$E_2 = \frac{1}{2}\left(\eta_{xx} + \eta_{yy} + \frac{1}{y}\eta_y\right) + (\eta_x^2 + \eta_y^2) - \frac{1}{2}\left(\frac{Re\,Pr}{2}\eta_x u + \frac{Re\,Pr}{2}\eta_y v\right)$$

$$E_3 = -\frac{1}{2}\left(\xi_{xx} + \xi_{yy} + \frac{1}{y}\xi_y\right) + (\xi_x^2 + \xi_y^2) + \frac{1}{2}\left(\frac{Re\,Pr}{2}\xi_x u + \frac{Re\,Pr}{2}\xi_y v\right)$$

$$E_4 = -\frac{1}{2}\left(\eta_{xx} + \eta_{yy} + \frac{1}{y}\eta_y\right) + (\eta_x^2 + \eta_y^2) + \frac{1}{2}\left(\frac{Re\,Pr}{2}\eta_x u + \frac{Re\,Pr}{2}\eta_y v\right)$$

$$E_5 = \frac{1}{2}(\xi_x\eta_x + \xi_y\eta_y). \tag{26}$$

In the present study, a hybrid scheme is used. Under the hybrid scheme, central difference is utilized when

$$|Re_{\Delta\xi}| \leqslant 2 \quad \text{and} \quad |Re_{\Delta\eta}| \leqslant 2 \quad \text{for equation (23)}$$

and

$$|Pe_{\Delta\xi}| \leqslant 2 \quad \text{and} \quad |Pe_{\Delta\eta}| \leqslant 2 \quad \text{for equation (25)}$$

where

$$Re_{\Delta\xi} = \frac{\left(\xi_{xx}+\xi_{yy}+\frac{1}{y}\xi_y\right)-\left(\frac{Re}{2}\xi_x u+\frac{Re}{2}\xi_y v\right)}{(\xi_x^2+\xi_y^2)}$$

$$Re_{\Delta\eta} = \frac{\left(\eta_{xx}+\eta_{yy}+\frac{1}{y}\eta_y\right)-\left(\frac{Re}{2}\eta_x u+\frac{Re}{2}\eta_y v\right)}{(\eta_x^2+\eta_y^2)}$$

$$Pe_{\Delta\xi} = \frac{\left(\xi_{xx}+\xi_{yy}+\frac{1}{y}\xi_y\right)-\left(\frac{Re\,Pr}{2}\xi_x u+\frac{Re\,Pr}{2}\xi_y v\right)}{(\xi_x^2+\xi_y^2)}$$

$$Pe_{\Delta\eta} = \frac{\left(\eta_{xx}+\eta_{yy}+\frac{1}{y}\eta_y\right)-\left(\frac{Re\,Pr}{2}\eta_x u+\frac{Re\,Pr}{2}\eta_y v\right)}{(\eta_x^2+\eta_y^2)} \tag{27}$$

Outside these ranges, the upwind difference is used with the diffusion terms ($\omega_{\xi\xi}$, $\omega_{\eta\eta}$, $T_{\xi\xi}$, $T_{\eta\eta}$) set equal to zero. The coefficients in equations (23) and (25) become

$$D_0 = \frac{Re}{2}\xi_x(A_1+A_2)+\frac{Re}{2}\eta_y(B_1+B_2)-\frac{Re\,v}{2y}+\frac{1}{y^2}$$

$$D_1 = \frac{1}{2}\left(\xi_{xx}+\xi_{yy}+\frac{1}{y}\xi_y\right)+\frac{Re}{2}\xi_x A_2-\frac{Re}{4}\xi_y v$$

$$D_2 = \frac{1}{2}\left(\eta_{xx}+\eta_{yy}+\frac{1}{y}\eta_y\right)+\frac{Re}{2}\eta_x B_2-\frac{Re}{4}\eta_x v$$

$$D_3 = -\frac{1}{2}\left(\xi_{xx}+\xi_{yy}+\frac{1}{y}\xi_y\right)+\frac{Re}{2}\xi_x A_1+\frac{Re}{4}\xi_y v$$

$$D_4 = -\frac{1}{2}\left(\eta_{xx}+\eta_{yy}+\frac{1}{y}\eta_y\right)+\frac{Re}{2}\eta_y B_1+\frac{Re}{4}\eta_x u$$

$$D_5 = \frac{1}{2}(\xi_x\eta_x+\xi_y\eta_y) \tag{28}$$

and

$$E_0 = \frac{Re\,Pr}{2}\xi_x(A_1+A_2)+\frac{Re\,Pr}{2}\eta_y(B_1+B_2)$$

$$E_1 = \frac{1}{2}\left(\xi_{xx}+\xi_{yy}+\frac{1}{y}\xi_y\right)+\frac{Re\,Pr}{2}\xi_x A_2-\frac{Re\,Pr}{4}\xi_y v$$

$$E_2 = \frac{1}{2}\left(\eta_{xx}+\eta_{yy}+\frac{1}{y}\eta_y\right)+\frac{Re\,Pr}{2}\eta_y B_2-\frac{Re\,Pr}{4}\eta_x u$$

$$E_3 = -\frac{1}{2}\left(\xi_{xx}+\xi_{yy}+\frac{1}{y}\xi_y\right)+\frac{Re\,Pr}{2}\xi_x A_1+\frac{Re\,Pr}{4}\xi_y v$$

$$E_4 = -\frac{1}{2}\left(\eta_{xx}+\eta_{yy}+\frac{1}{y}\eta_y\right)+\frac{Re\,Pr}{2}\eta_y B_1+\frac{Re\,Pr}{4}\eta_x u$$

$$E_5 = \frac{1}{2}(\xi_x\eta_x+\xi_y\eta_y) \tag{29}$$

where

$$A_1 = [|u,0|]$$
$$A_2 = [|-u,0|]$$
$$B_1 = [|v,0|]$$
$$B_2 = [|-v,0|]. \tag{30}$$

Equations (21), (23) and (25) form a set of nonlinear algebraic equations which can be solved by an iteration scheme. A line by line successive underrelaxation method is used.

5. RESULTS AND DISCUSSION

Numerical solutions have been obtained for a three-droplet array. The results obtained from an earlier study [3] and those from Tal *et al.* [1] have been used for comparison and are shown in Figs. 6–8. It is

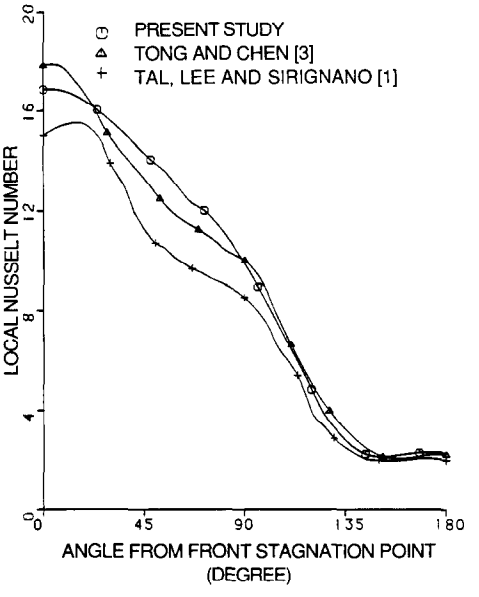

FIG. 6. Local Nusselt number comparison for the first droplet of a three-droplet array: $b/a = 1.5$, $Re = 100$, $Pr = 1$.

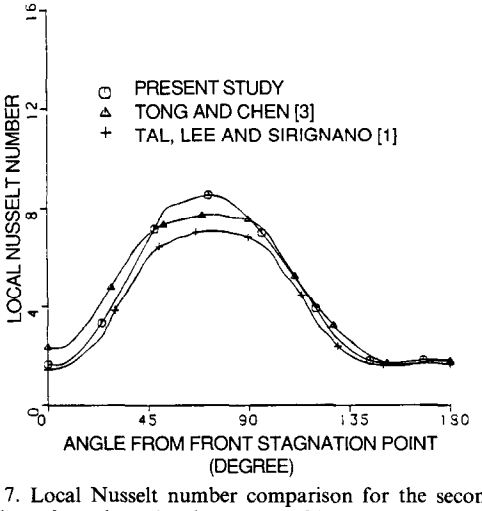

FIG. 7. Local Nusselt number comparison for the second droplet of a three-droplet array: $b/a = 1.5$, $Re = 100$, $Pr = 1$.

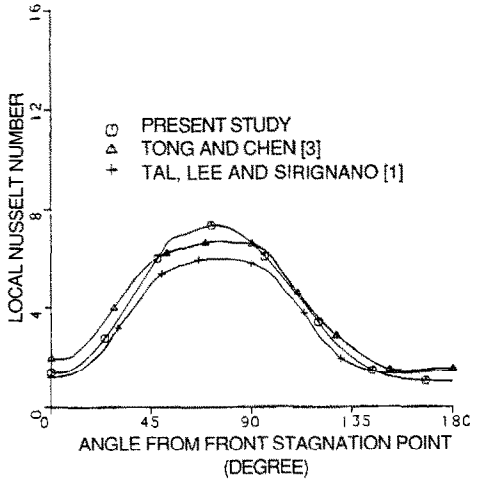

FIG. 8. Local Nusselt number comparison for the third droplet of a three-droplet array: $b/a = 1.5$, $Re = 100$, $Pr = 1$.

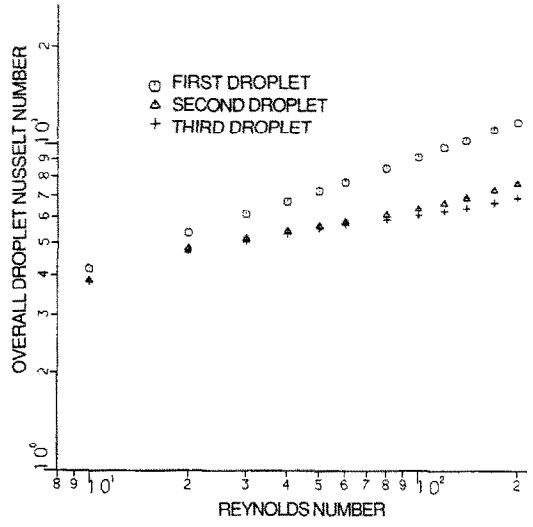

FIG. 9. Overall droplet Nusselt number for a non-vaporizing three-droplet array: $b/a = 1.5$, $Pr = 1$.

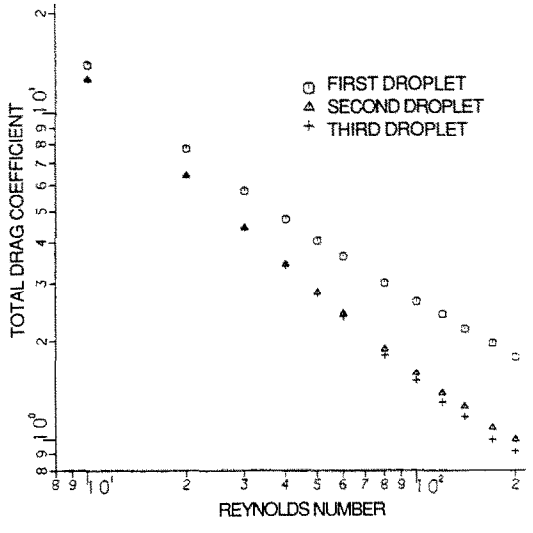

FIG. 10. Total drag coefficient for a non-vaporizing three-droplet array: $b/a = 1.5$, $Pr = 1$.

interesting to note that in the results of Tal *et al.* [1] the maximum heat transfer for the first droplet is not located at the stagnation point. No discussion about the dip in local Nusselt number at the stagnation point is given in Tal *et al.* [1]. On the other hand, the local Nusselt number for the first droplet obtained by the present authors decreases monotonically from the stagnation point region to the shoulder region and then becomes negligibly small in the separation region. This is also observed in single droplet analyses by Renksizbulut and Yuen [9] and by Sayegh and Gauvin [10]. Although discrepancy of Nusselt number behavior at the frontal stagnation point exists, the contribution of the stagnation point to the overall heat transfer is negligible because of the relatively limited extent of area involved. For the second and third droplet, the front region of the droplet contains wakes due to the flow separation from the rear region of the droplet upstream. The heat transfer rate in the front region of the droplet is severely decreased.

It should be mentioned that the Nusselt numbers for all three droplets obtained by the present authors, both in the present study and in the previous work [3], are higher than those obtained by Tal *et al.* [1]. In ref. [3], the results for the non-vaporizing single droplet case show that the hybrid scheme yields better agreement with the results from ref. [9], and the upwind difference scheme used in ref. [1] yields lower values.

As typical for any iteration scheme, the number of iterations for convergence depends on the initial guess. In the present study, the result for the $Re = 10$ case is used as the initial guess for the $Re = 20$ case. The iteration process is marching forward with a Reynolds number increment of 10 after each convergence.

The mesh used in the present study (Fig. 3) consists of a 91×21 grid with three large empty squares embedded corresponding to the three droplets. The following relaxation factors are used in the calculations: 0.35 for ω; 0.9 for both ψ and T. It consumes about 7.5 min of CPU time on an IBM-4341 system to reach the solution for $Re = 100$ by the marching scheme mentioned above with less than 0.1% convergence error. The corresponding CPU time consumed in the previous study [3] is about 20 min. The amount of CPU time for the grid generation is about 1.5 min.

The results for the overall Nusselt number and total drag coefficient as a function of Reynolds number are shown in Figs. 9 and 10, respectively. The values of the drag coefficient as well as Nusselt number for the first droplet are distinctively higher than the values for the two downstream droplets. This result is in compliance with the study of Tal *et al.* [1]. The figures show that the results for the second droplet resemble the results for the third droplet. This suggests that

periodic behavior can be expected after the first droplet.

Attempts have been made to search for experimental results which can be used for comparison with the numerical results. Unfortunately, due to the geometry constraints used in the present work, no experimental results have been found in the existing literature which are useful for comparison.

6. SUMMARY

The use of a grid generation technique for the numerical solution of heat transfer and hydrodynamics in a three-droplet array has been developed. The Navier–Stokes equation in vorticity–stream-function form and the energy equation have been solved. Numerical solutions have been obtained for the Reynolds number range of 10–200. The results are compared with the results obtained in an earlier study as well as those in the literature. The body-fitted coordinates presented in this study require less computer time than the earlier study [3] and are more suitable for treating the more general problem of droplet heating and vaporization. Due to the geometry concerned in the present study, no experimental result can be found in the existing literature for comparison.

Acknowledgement—The authors wish to acknowledge support of this research by the National Science Foundation under research grant MEA-8404292.

REFERENCES

1. R. Tal, D. N. Lee and W. A. Sirignano, Hydrodynamics and heat transfer in sphere assemblages—cylindrical cell models, *Int. J. Heat Mass Transfer* **26,** 1265–1273 (1983). Also see ASME Preprint 81-WA/HT-44 (1981) and AIAA Preprint 82-0302 (1982).
2. R. Tal, D. N. Lee and W. A. Sirignano, Periodic solutions of heat transfer for flow through a periodic assemblage of spheres, *Int. J. Heat Mass Transfer* **27,** 1414–1417 (1984).
3. A. Y. Tong and S. J. Chen, Heat transfer correlations for vaporizing liquid droplet arrays in a high temperature gas at intermediate Reynolds number, *Int. J. Heat Fluid Flow* (1988), in press. Also see Fall Technical Meeting, Eastern Section of the Combustion Institute, San Juan, Puerto Rico, December (1986).
4. G. A. Patnaik, A numerical solution of droplet vaporization with convection, Ph.D. Thesis, Carnegie-Mellon University, Pittsburgh, Pennsylvania (1986).
5. J. F. Thompson, F. C. Thames and C. W. Mastin, Automatic numerical generation of body-fitted curvilinear coordinate system for field containing any number of arbitrary two-dimensional bodies, *J. Computational Phys.* **25,** 299–319 (1974).
6. J. F. Thompson, Z. U. A. Warsi and C. W. Mastin, *Numerical Grid Generation—Foundations and Applications*. Elsevier, Amsterdam (1985).
7. S. Prakash, Unsteady theory of droplet vaporization with large gas and liquid Reynolds number, Ph.D. Thesis, Princeton University, Princeton, New Jersey (1978).
8. V. G. Jenson, Viscous flow round a sphere at low Reynolds number (<40), *Proc. R. Soc. (London)* **249A,** 346–366 (1959).
9. M. Renksizbulut and M. C. Yuen, Numerical study of droplet evaporation in a high-temperature stream, *ASME J. Heat Transfer* **105**(2), 389–397 (1983).
10. N. N. Sayegh and W. H. Gauvin, Numerical analysis of variable property heat transfer to a single sphere in high temperature surroundings, *A.I.Ch.E. Jl* **25,** 522–534 (1979).

APPLICATION DE LA TECHNIQUE DE GENERATION DE GRILLE ELLIPTIQUE A LA RESOLUTION DE L'HYDRODYNAMIQUE ET DU TRANSFERT THERMIQUE POUR DES GOUTTELETTES A DES NOMBRES DE REYNOLDS INTERMEDIAIRES

Résumé—On emploie la technique de génération d'une grille numérique à la résolution de l'hydrodynamique et du transfert thermique dans un arrangement à trois gouttalettes. Des équations aux dérivées partielles elliptiques sont utilisées pour obtenir des grilles dans le plan physique. Les équations de Navier–Stokes dans la forme vorticité–fonction de courant et l'équation d'énergie sont résolues numériquement par la méthode des différences finies pour des nombres de Reynolds variant entre 10 et 200. Des solutions numériques sont obtenues en terme de coefficient de trainée et de nombre de Nusselt. Les résultats sont comparés à ceux obtenus dans une étude antérieure et à d'autres tirés de la bibliographie.

DIE ANWENDUNG EINER ELLIPTISCHEN NETZGENERIERUNGSTECHNIK AUF DIE UNTERSUCHUNG VON HYDRODYNAMIK UND WÄRMEÜBERTRAGUNG VON TROPFENSCHWÄRMEN BEI MÄSSIGEN REYNOLDS-ZAHLEN

Zusammenfassung—Das Ziel der vorliegenden Arbeit ist es, eine numerische Netzgenerierungstechnik zur Untersuchung von Hydrodynamik und Wärmeübertragung eines Drei-Tropfen-Schwarms anzuwenden. Elliptische partielle Differentialgleichungen werden benutzt, um die Netze in der physikalischen Ebene zu generieren. Die Navier–Stokes-Gleichungen in der Form Wirbeltransport–Stromfunktion und die Energiegleichungen wurden mit einem Finite-Differenzen-Verfahren für Reynolds-Zahlen von 10 bis 200 gelöst. Numerische Lösungen wurden in Form von Reibungskoeffizienten und Nusselt-Zahlen ermittelt. Die Ergebnisse wurden mit solchen aus früheren Untersuchungen und mit Literaturwerten verglichen.

ПРИМЕНЕНИЕ МЕТОДА ГЕНЕРИРОВАНИЯ ЭЛЛИПТИЧЕСКИХ СЕТОК ДЛЯ РЕШЕНИЯ ЗАДАЧ ГИДРОДИНАМИКИ И ТЕПЛОПЕРЕНОСА В КАПЕЛЬНЫХ ФАКЕЛАХ ПРИ ПРОМЕЖУТОЧНЫХ ЗНАЧЕНИЯХ ЧИСЛА РЕЙНОЛЬДСА

Аннотация—Целью настоящего исследования являлось применение метода численной сеточной генерации для решения задач гидродинамики и тепдообмена в факеле капель трёх типов. Используются эллиптические дифференциальные уравнения в частных производных для генерирования сеток в физической плоскости. Уравнения Навье–Стокса, записанные в форме завихренности и функции тока, и уравнение энергии решались численно методом конечных разностей для диапазона числа Рейнольдса от 10 до 200. Численные решения получены в виде коэффициента сопротивления и числа Нуссельта. Результаты сравниваются с данными, полученными в ранее проведённом исследовании и представленными в литературе.